**TELKOMNIKA Telecommunication Computing Electronics and Control**
Vol. 24, No. 3, June 2026, pp. 1068~1082
ISSN: 1693-6930, DOI: 10.12928/TELKOMNIKA.v24i3.27270 

# Experimental modeling of a square planar micro-coil

**Assia Ouali[1], Fatima Zohra Medjaoui[1], Azzedine Hamid[1,2], Mohamed Rizouga[1], Abderrahim Mokhefi[3], Hocine Guentri[2]**
[1]Department of Electrotechnics, Faculty of Electrical Engineering, University of Science and Technology of Oran, USTO-MB, Oran, Algeria
[2]Department of Electrical Engineering, Institute of Technology, Nour El Bachir University Center, El Bayadh, Algeria
[3]Departement of Mechanical Engineering, National Polytechnic School of Oran Maurice Audin, Oran, Algeria

**Article Info**

***Article history:***

Received Jun 10, 2025
Revised Feb 4, 2026
Accepted Mar 29, 2026

***Keywords:***

Analytical modeling
Dimensional geometry
Experimental model
Interaction parameters
Planar spiral coils
Sising coil

**ABSTRACT**

This study focuses on developing miniaturized electromagnetic components for applications in integrated microsystems, magnetic sensors, contactless energy transfer, and compact power converters. In a context of miniaturization and the pursuit of greater energy efficiency, the planar micro-coil plays a key role due to its compact size, ease of integration, and compatibility with microfabrication technologies. The work presented explores the design, modeling, fabrication, and experimental characterization of a square planar micro-coil. Its electromagnetic properties, such as inductance, resistance, and quality factor, are highly dependent on factors like the coil's geometry (turns, track width, spacing, conductor thickness), substrate characteristics, and the manufacturing process. The main goal is to propose an accurate experimental model linking geometric parameters to electrical performance. The approach combines analytical modeling, finite element modeling (FEM), and experimental measurements on microfabricated prototypes. The results show strong agreement between theoretical predictions and experimental data, validating the model's relevance. Lastly, the study highlights the impact of skin effects, proximity effects, and ohmic losses on the coil's performance, offering insights for optimizing its design for high-performance, compact electromagnetic devices.



***Corresponding Author:***

Hocine Guentri
Department of Electrical Engineering, Institute of Technology, Nour El Bachir University Center
El Bayadh, Algeria
Email: h.guentri@cu-elbayadh.dz

## 1. INTRODUCTION

The continuous miniaturization of electronic systems imposes increasingly stringent constraints on the design of passive components, particularly in terms of compactness, electromagnetic performance, and compatibility with microfabrication processes. In this context, planar micro-coils are key components in numerous applications, including integrated microsystems, magnetic sensors, wireless power transfer, and miniaturized power converters [1], [2]. Although analytical and numerical approaches, such as finite element method (FEM) simulations, are widely employed to estimate their electromagnetic characteristics, systematic experimental validation remains limited, especially for square planar micro-coils [3], [4].

Conventional analytical models exhibit significant limitations when applied at the micrometer scale, where the performance of planar micro-coils arises from complex interactions among multiple geometrical parameters, including track width, inter-turn spacing, conductor thickness, and outer diameter [5], [6]. These parameters cannot be considered independently, as their combined effects strongly influence key

performance metrics such as inductance, series resistance, and quality factor. The lack of a structured experimental methodology capable of simultaneously quantifying main effects and interaction effects constitutes a major obstacle to the reliable optimization of planar micro-coils.

The design of experiments (DOE) methodology provides a rigorous and efficient framework to address this challenge. By carefully selecting key geometrical factors and their corresponding levels, DOE enables a systematic exploration of the design space while significantly reducing the number of fabricated samples, which is particularly critical in a microfabrication context. Furthermore, the associated statistical analysis makes it possible to identify not only dominant main effects but also significant interactions between parameters, which are often overlooked in purely analytical or numerical approaches.

In this work, a DOE-based approach is implemented to establish a predictive experimental model of the electromagnetic performance of square planar micro-coils, validated through precise experimental measurements [7]–[9]. This methodology allows the sensitivity of coil performance to geometrical variations to be quantified and enables an assessment of design robustness with respect to process-induced variations inherent to microfabrication technologies. The experimental results exhibit a strong correlation with theoretical predictions, while also revealing nonlinear behaviors and interaction effects, particularly associated with the outer diameter, which play a critical role in optimizing high-frequency performance [8], [10]. The proposed DOE-based approach thus constitutes a powerful tool for the robust and optimized design of planar micro-coils intended for advanced microelectronic applications.

## 2. USING EXPERIMENTAL DESIGN TO EVALUATE PLANAR MICRO-COILS PERFORMANCE

### 2.1. Presentation of the planar micro-coil

#### 2.1.1. Simulation setup and device description

A square planar spiral micro-coil deposited on a multilayer substrate was selected for this study, as shown in Figure 1. The objective is to integrate this planar micro-coil into a low-power, low-voltage buck direct current (DC)–DC converter [2], [3]. The main challenge associated with this integration lies in the development of an accurate sizing and modeling methodology for the planar micro-coil that ensures minimal losses under high-frequency operating conditions. The electromagnetic behavior of the micro-coil was analyzed using computer solution (COMSOL) Multiphysics, based on three-dimensional finite element simulations.

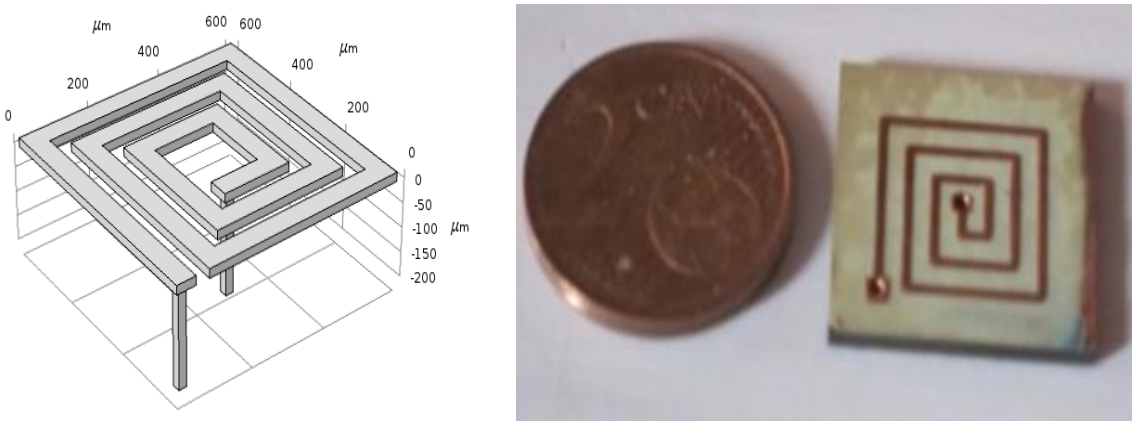


Figure 1. Square micro-coil on kapton and ferrite substrate

#### 2.1.2. Boundary conditions

The electromagnetic simulations were performed using the alternating current (AC)/DC module of COMSOL Multiphysics, assuming frequency-domain operation. To emulate an open-boundary environment and avoid artificial field confinement, appropriate boundary conditions were applied to the outer surfaces of the computational domain. In particular, magnetic insulation conditions were imposed on selected boundaries, while infinite element domains were employed to effectively truncate the simulation space and accurately model the radiation of electromagnetic fields. This combination ensures reliable field distribution and precise extraction of impedance-related parameters.

### 2.1.3. Meshing strategy

The accuracy of the finite element simulations strongly depends on the mesh quality, especially at high frequencies. A non-uniform adaptive meshing strategy was adopted, with local mesh refinement in regions exhibiting high electromagnetic field gradients, namely the conductive tracks of the micro-coil, the inter-turn gaps, and the conductor–substrate interfaces. In COMSOL Multiphysics, higher-order tetrahedral elements were used within the conductors to accurately capture current crowding, skin, and proximity effects. Mesh convergence studies were systematically conducted to ensure that the extracted electromagnetic parameters were independent of the mesh density.

### 2.1.4. Frequency sweep

A frequency-domain analysis was carried out over a range compatible with the target application. A parametric frequency sweep was performed around the nominal operating frequency of the buck converter, set to 500 kHz, in order to evaluate the frequency-dependent behavior of the micro-coil. Key performance metrics such as inductance, series resistance, and quality factor were extracted as functions of frequency. The frequency step was selected to provide sufficient resolution to capture frequency-dependent loss mechanisms, particularly skin and proximity effects, which are critical for high-frequency operation.

### 2.1.5. Converter topology and electrical specifications

The converter topology was deliberately kept simple, as the objective of this work is not to propose a novel power conversion architecture, but to rely on a well-established buck converter that can be integrated with minimal complexity. Nevertheless, the selected topology inherently requires the integration of a micro-coil, which constitutes the key component under investigation [4], [5]. The structure of the considered buck converter is shown in Figure 2. The electrical specifications of the converter are: input voltage ($Ve = 5$ V), output voltage ($Vs = 2.5$ V), output power ($Ps = 1$ W), operating frequency ($f = 500$ kHz), and duty cycle ($\mathrm{D} = \mathrm{Vs}/\mathrm{Ve} = 0.5$).

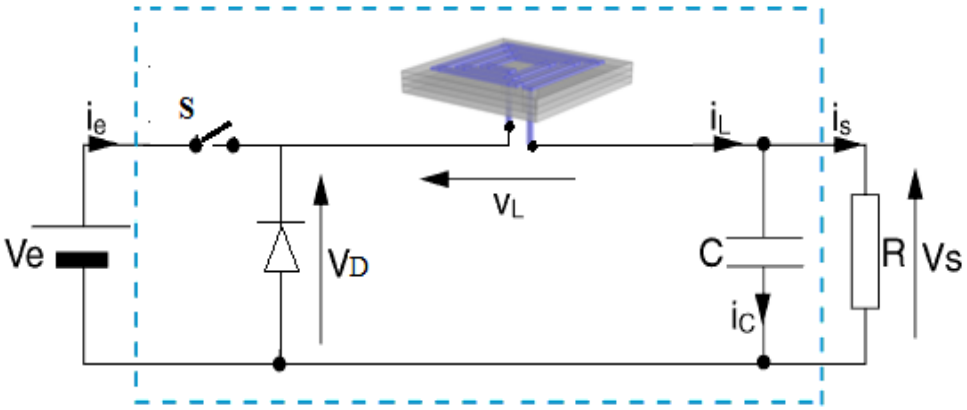


Figure 2. Schematic of a buck DC-DC converter containing the square spiral planar micro-coil

The planar micro-coil is governed by several parameters, which can be grouped into two main classes. In this study, we focus on the inter-turn spacing s, the conductor width t, the thickness w and the number of turns n. Together, these parameters constitute a set of factors that define the dimensional characteristics of the planar micro-coil. The interactions between these factors can be investigated using a design of experiments approach [9], [10].

The selection of appropriate levels for each factor is crucial, as it determines the experimental domain within which the conclusions drawn from the study remain valid [11]–[14]. The experimental domain considered in this work enables the construction of the experimental matrix, as presented in Table 1. Given that four factors are examined at two levels each, a full factorial design is adopted as the initial step in the analysis. This design is well suited for modeling purposes, as it allows the development of first-order models that include interaction effects between factors [2], [4].

Table 1. Experimental domain

| Factors | Min. values | Max. values |
|---|---|---|
| Turns spacings (µm) | 0.5 | 2.5 |
| Width $t$ (µm) | 0.1 | 0.5 |
| Thickness $w$ (µm) | 1.8 | 90 |
| Number of turns ($n$) | 2 | 16 |

## 3. EXPERIMENTAL PROCEDURE

The proposed theoretical model was validated through a systematic experimental characterization of square planar micro-coils with varying geometrical parameters. The investigated factors include conductor width ($w$), thickness, inter-turn spacing, and outer diameter ($d_{out}$). The experimental campaign was designed using a DOE methodology in order to quantify both main effects and interaction effects on the electrical characteristics of the micro-coils, with particular emphasis on inductance.

Electrical measurements were performed using an impedance analyzer over a frequency range centered around 500 kHz, corresponding to the intended operating conditions of the integrated DC–DC converter. Each micro-coil was measured individually using short, low-parasitic connections to minimize lead effects. Prior to the measurements, the impedance analyzer was calibrated using an open–short–load (OSL) procedure at the probe reference plane. This calibration ensured the compensation of systematic errors associated with cables, connectors, and measurement fixtures. Residual lead inductance and resistance were further evaluated through reference open and short measurements and were subtracted from the raw data.

Parasitic capacitances arising from the substrate, inter-turn coupling, and measurement interconnections were taken into account through frequency-domain analysis. The complex impedance data were interpreted using an equivalent resistor–inductor–capacitor (RLC) model, allowing the extraction of the inductive component in the frequency region where inductive behavior dominates. Only measurements within this region were retained for parameter identification. The experimental results were analyzed and presented primarily in graphical form to facilitate the interpretation of trends and interactions between geometrical parameters. A strong agreement was observed between experimental data, analytical predictions, and simulation results, confirming the validity of the proposed modeling approach at the micrometer scale.

### 3.1. Experimentations results

The experimental setup used in this study makes it possible to evaluate the inductance ($L$) as a function of the turn spacing ($s$), conductor width ($t$), thickness ($w$) and outer diameter ($d_{out}$). Each experimental point corresponds to the average value obtained from approximately twenty measurements, thereby improving measurement reliability. In the present work, particular attention is devoted to face-centred composite designs (FCC), which are well suited for modeling using response surface methodology (RSM) [15]–[18]. The main advantage of the FCC design lies in its sequential nature: the process is initially modelled using a first-order polynomial. Accordingly, the first step of this study consists in establishing a full factorial experimental design. If the resulting linear model is validated, the experimental campaign is terminated. Otherwise, the analysis is extended to a second-order polynomial model through the construction of a composite face-centred design. The results obtained from the 19 experimental runs of the full factorial design are reported in Table 2.

### 3.2. Results of the full factorial plan

Table 2 presents the estimated values obtained using the mathematical model established by the experimental design methodology applying the MODDE 05 software. These are compared with the values measured according to the centred factorial design. We will carry out this calculation using the classical method; it should be remembered that the matrix method can also be used, but in both cases the mathematical model is that associated with factorial plans.

#### 3.2.1. Matrix for calculating effects

Table 3 presents the matrix for calculating reduced effects using the high, low and central levels dictated by the experimental design methodology. Each result in the last column of the table is the result of using the levels of our experimental design according to the mathematical model.

$$Y = a_0 + a_n * n + a_{dout} * dout + a_w * w + a_s * s + a_{n-dout} * nd_{out} + a_{n-w} * nw + a_{n-s} * ns + a_{dout-w} * d_{out}w + a_{dout-s} * d_{out}s + a_{w-s}ws \quad (1)$$

Table 2. Results of the full factorial plan

| EXP no | $n$ | $d_{out}$ | $w$ | $s$ | $L_{est}$ | $L$ |
|---|---|---|---|---|---|---|
| 1 | 2 | 145 | 1.8 | 0.8 | -0.00992723 | 1.557 e-5 |
| 2 | 16 | 145 | 1.8 | 0.8 | -0.000742769 | 0.0092 |
| 3 | 2 | 532 | 1.8 | 0.8 | -0.00992719 | 1.557 e-5 |
| 4 | 16 | 532 | 1.8 | 0.8 | -0.000742754 | 0.0092 |
| 5 | 2 | 145 | 90 | 0.8 | -0.00930297 | 0.0006398 |
| 6 | 16 | 145 | 90 | 0.8 | 0.318857 | 0.3288 |
| 7 | 2 | 532 | 90 | 0.8 | -0.009303 | 0.0006398 |
| 8 | 16 | 532 | 90 | 0.8 | 0.318857 | 0.3288 |
| 9 | 2 | 145 | 1.8 | 18 | -0.00986632 | 7.6436 e-5 |
| 10 | 16 | 145 | 1.8 | 18 | 0.0577572 | 0.0677 |
| 11 | 2 | 532 | 1.8 | 18 | -0.0098663 | 7.6436 e-5 |
| 12 | 16 | 532 | 1.8 | 18 | 0.0577573 | 0.0677 |
| 13 | 2 | 145 | 90 | 18 | -0.00924214 | 0.00070066 |
| 14 | 16 | 145 | 90 | 18 | 0.377357 | 0.3873 |
| 15 | 2 | 532 | 90 | 18 | -0.00924216 | 0.00070066 |
| 16 | 16 | 532 | 90 | 18 | 0.377357 | 0.3873 |
| 17 | 9 | 338.5 | 45.9 | 9.4 | 0.0893613 | 0.035 |
| 18 | 9 | 338.5 | 45.9 | 9.4 | 0.0893613 | 0.038 |
| 19 | 9 | 338.5 | 45.9 | 9.4 | 0.0893613 | 0.036 |

Table 3. Effects calculation matrix

| $a_0$ | $n$ | $d_{out}$ | $w$ | $s$ | $I_{n-dout}$ | $I_{n-w}$ | $I_{n-s}$ | $I_{dout-w}$ | $I_{dout-s}$ | $I_{w-s}$ | $L_{est}(H)$ |
|---|---|---|---|---|---|---|---|---|---|---|---|
| 1 | -1 | -1 | -1 | -1 | +1 | +1 | +1 | +1 | +1 | +1 | 1.557 e-5 |
| 1 | 1 | -1 | -1 | -1 | -1 | -1 | -1 | +1 | +1 | +1 | 0.0092 |
| 1 | -1 | 1 | -1 | -1 | -1 | +1 | +1 | -1 | -1 | +1 | 1.557 e-5 |
| 1 | 1 | 1 | -1 | -1 | +1 | -1 | -1 | -1 | -1 | +1 | 0.0092 |
| 1 | -1 | -1 | 1 | -1 | +1 | -1 | +1 | -1 | +1 | -1 | 0.000639 |
| 1 | 1 | -1 | 1 | -1 | -1 | +1 | -1 | -1 | +1 | -1 | 0.3288 |
| 1 | -1 | 1 | 1 | -1 | -1 | -1 | +1 | +1 | -1 | -1 | 0.000639 |
| 1 | 1 | 1 | 1 | -1 | +1 | +1 | -1 | +1 | -1 | -1 | 0.3288 |
| 1 | -1 | -1 | -1 | 1 | +1 | +1 | -1 | +1 | -1 | -1 | 7.6436 e-5 |
| 1 | 1 | -1 | -1 | 1 | -1 | -1 | +1 | +1 | -1 | -1 | 0.0677 |
| 1 | -1 | 1 | -1 | 1 | -1 | +1 | -1 | -1 | +1 | -1 | 7.6436 e-5 |
| 1 | 1 | 1 | -1 | 1 | +1 | -1 | +1 | -1 | 1 | -1 | 0.0677 |
| 1 | -1 | -1 | 1 | 1 | +1 | -1 | -1 | -1 | -1 | +1 | 0.000700 |
| 1 | 1 | -1 | 1 | 1 | -1 | 1 | +1 | -1 | -1 | +1 | 0.3873 |
| 1 | -1 | 1 | 1 | 1 | -1 | -1 | -1 | +1 | +1 | +1 | 0.0007006 |
| 1 | 1 | 1 | 1 | 1 | 1 | 1 | +1 | 1 | 1 | 1 | 0.3873 |
| 1 | 0 | 0 | 0 | 0 | 0 | 0 | 0 | 0 | 0 | 0 | 0.035 |
| 1 | 0 | 0 | 0 | 0 | 0 | 0 | 0 | 0 | 0 | 0 | 0.038 |
| 1 | 0 | 0 | 0 | 0 | 0 | 0 | 0 | 0 | 0 | 0 | 0.036 |

## 4. DETERMINATION OF INDUCTANCE VALUE

### 4.1. Study domain

The selection of levels assigned to each factor is a crucial step in the design of the experiment. Indeed, these levels determine the domain of study within which the obtained results can be interpreted and applied. As illustrated in Table 4, an appropriate choice ensures the validity and relevance of the conclusions drawn from the experiment. The choice of the levels of each factor is essential because it defines the field of study within which the conclusions of the experiment will be valid, as in Table 4.

Table 4. Study domain [5], [6]

| | n | $d_{out}$(µm) | w (µm) | s (µm) |
|---|---|---|---|---|
| Level (-) | 2 | 145 | 20 | 2 |
| Level (0) | 9 | 338.5 | 23 | 4 |
| Level (+) | 16 | 532 | 26 | 6 |

### 4.2. Setting up the mathematical model

The $a_o$ is a constant, the value of the response at the centre of the domain. In the case of factorial designs with the experimental points located at the vertices of the study domain, this constant is the average of all the responses, this gives (2):

$$a_0 = \frac{\sum_{i=1}^{i=19}(I_p)i}{n} = \frac{1.557e^{-0.05}+0.0092+\cdots+0.036}{19} = 0.0893613H \quad (2)$$

The effect of the number of turns ($a_n$) is calculated by multiplying each response by the value of the sign in the column for factor 1 ($n$). i.e., Ip1 by -1. Ip2 by +1. Ip3 by -1 and so on. Kindly remember that the points at the centreare not taken into account when calculating effects and interactions. We can therefore set the (3):

$$a_n = \frac{-y1+y2-y3+\cdots+y19}{16} = 0.0989459H \quad (3)$$

The same procedure is adopted for the effects and interactions of the other factors.

$$\textit{Effect of external diameter } d_{out} a_{dout} = \frac{-y1-y2+y3+\cdots+y19}{16} = -1.02897e^{-3}H \quad (4)$$

$$\textit{Effect of the width } w a_w = \frac{-y1-y2-y3-y4\ldots+y19}{16} = 0.0800561\ H \quad (5)$$

$$\textit{Effect of Inter-turns } s\ a_s = \frac{-y1-y2-\cdots-y8+\cdots+y19}{16} = 0.0146402\ H \quad (6)$$

We proceed to calculate the effects of interactions between factors. Interaction between the number of turns and the external diameter ($I_{n-dout}$)*:* is calculated by multiplying each response by the value of the sign shown in the 6th column. i.e., $Ip_1$ by +1. $Ip_2$ by -1. $Ip_3$ by -1 and so on. The same procedure is adopted for other interactions as in (8)-(12).

$$I_{n-dout} = \frac{+l1-l2-l3+y4+\cdots+l19}{16} = 2.0063e^{-3}H \quad (7)$$

Interaction between turns number $n$ and the width $w$:

$$I_{n-w} = \frac{+l1-l2+l3-\cdots+l19}{16} = 8.6545e^{-2}H \quad (8)$$

Interaction between turns number of *n* and the inter-turns $s$:

$$I_{n-s} = \frac{+l1-l2+-\cdots+l19}{16} = 1.2967\mathrm{e}^{-2}H \quad (9)$$

Interaction between the external diameter $d_{out}$ and the width *w*:

$$I_{dout-w} = \frac{+l1+l2-l3\ldots+l19}{16} = 1.1618e^{-2}H \quad (10)$$

Interaction between the external diameter $d_{out}$ and the inter-turns $s$:

$$I_{dout-s} = \frac{+l1+l2-l3-l4\ldots+l19}{16} = 1.1618e^{-2} \quad (11)$$

Interaction between width *w* and inter-turns *s*:

$$I_{w-s} = \frac{+l1+l2+l3+l4-\cdots+l19}{16} = 1.5282\mathrm{e}^{-2}H \quad (12)$$

The mathematical model of the inductance *L* can therefore be expressed by the (13).

$$L = 0.0893613 + 0.0989459 * n - 1.02897e^{-8} * d_{out} + 0.0800561 * w + 0.0146402 * s + 2.13323e^{-9} * nd_{out} + 0.0797439 * nw + 0.0146098 * ns + 5.96874e^{-11} * d_{out}w + (-)5.87277e^{-9}d_{out}s + 4.667e^{-9} * ws \quad (13)$$

### 4.3. Estimation of variance

Once the mathematical model we are looking for has been established, we now need to assess the quality of the model. To do this, we carry out an analysis of variance [19]–[22]. Using (2) to (13), this first step results in the construction of Table 5. From (15)-(17) of the statistical analysis of the model as a whole we have:

Table 5. Estimation of model effects

| N | $d_{out}$ | w | s | n×$d_{out}$ | n×w | n×s | $d_{out}$×w | $d_{out}$×s | w×s | Y | $Y_{est}$ | SCM | SCE | SCT |
|---|---|---|---|---|---|---|---|---|---|---|---|---|---|---|
| -1 | -1 | -1 | -1 | 1 | 1 | 1 | 1 | 1 | 1 | 1.557e$^{-5}$ | 1.55e$^{-5}$ | 0.0798 | 0 | 0.0798 |
| 1 | -1 | -1 | -1 | -1 | -1 | -1 | 1 | 1 | 1 | 0.0092 | 0.009 | 0.7811 | 0.0067 | 0.788 |
| -1 | 1 | -1 | -1 | -1 | 1 | 1 | -1 | -1 | 1 | 1.557e$^{-5}$ | 1.57e$^{-5}$ | 0.0798 | 1.44e-$^{14}$ | 0.0798 |
| 1 | 1 | -1 | -1 | 1 | -1 | -1 | -1 | -1 | 1 | 0.0092 | 0.0098 | 0.7811 | 0.0067 | 0.788 |
| -1 | -1 | 1 | -1 | 1 | -1 | + | -1 | 1 | -1 | 0.0064 | 0.0007 | 0.0787 | 6.4e$^{-11}$ | 0.078 |
| 1 | -1 | 1 | -1 | -1 | 1 | -1 | -1 | 1 | -1 | 0.3288 | 0.3488 | 0.0673 | 0.0004 | 0.067 |
| -1 | + | 1 | -1 | -1 | -1 | 1 | -1 | -1 | -1 | 0.0006 | 0.0007 | 0.0078 | 6.4e$^{-11}$ | 0.007 |
| 1 | 1 | 1 | -1 | 1 | 1 | -1 | 1 | -1 | -1 | 0.3288 | 0.3488 | 0.0673 | 0.0004 | 0.067 |
| -1 | -1 | -1 | 1 | 1 | 1 | -1 | 1 | -1 | -1 | 7.646e$^{-5}$ | 7.65e$^{-5}$ | 0.0079 | 1.1881e$^{-14}$ | 0.007 |
| 1 | -1 | -1 | 1 | -1 | -1 | 1 | 1 | -1 | -1 | 0.0677 | 0.0715 | 0.0003 | 1.444e$^{-5}$ | 0.0003 |
| -1 | 1 | -1 | 1 | -1 | 1 | -1 | -1 | 1 | -1 | 7.636e$^{-5}$ | 7.65e-5 | 0.0079 | 1.1881e$^{-14}$ | 0.008 |
| 1 | 1 | -1 | 1 | 1 | -1 | 1 | -1 | 1 | -1 | 0.0677 | 0.0735 | 0.0002 | 3.364e$^{-5}$ | 0.0028 |
| -1 | -1 | 1 | 1 | 1 | -1 | -1 | -1 | -1 | 1 | 0.000006 | 0.0007 | 0.0078 | 9.3702e$^{-11}$ | 0.0078 |
| 1 | -1 | 1 | 1 | -1 | 1 | 1 | -1 | -1 | 1 | 0.3873 | 0.3922 | 0.0917 | 2.401e$^{-5}$ | 0.0917 |
| -1 | 1 | 1 | 1 | -1 | -1 | -1 | 1 | 1 | 1 | 0.0007 | 0.0007 | 0.0078 | 8.723e$^{-11}$ | 0.00785 |
| 1 | 1 | 1 | 1 | + | 1 | 1 | 1 | 1 | 1 | 0.3873 | 0.3756 | 0.0819 | 0.1359 | 0.2178 |
| 0 | 0 | 0 | 0 | 0 | 0 | 0 | 0 | 0 | 0 | 0.0350 | 0.039 | 0 | 1.6e$^{-5}$ | 1.6e$^{-5}$ |
| 0 | 0 | 0 | 0 | 0 | 0 | 0 | 0 | 0 | 0 | 0.038 | 0.041 | 0 | 9e$^{-6}$ | 9e$^{-6}$ |
| 0 | 0 | 0 | 0 | 0 | 0 | 0 | 0 | 0 | 0 | 0.036 | 0.038 | 0 | 4e$^{-6}$ | 4e$^{-6}$ |

Knowing that:

$$\bar{Y} = \frac{\sum_1^{19} Y}{19} = 0.0896279 \tag{14}$$

$$SCM = \sum_{i=1}^{i=19} \left(\hat{Y} - \bar{Y}\right)^2 = 0.367779 \qquad SCE = \sum_{i=1}^{i=19} \left(Y_i - \hat{Y}\right)^2 = 0.010157$$
$$SCT = \sum_{i=1}^{i=19} (Y_i - \bar{Y})^2 = 0.377894 \tag{15}$$

### 4.4. Total variance (variance of residuals)

The residual variance is defined by equation (16). This equation represents the variation in the data that is not explained by the model used. It thus allows for the evaluation of the gap between the observed values and the predicted values, representing the portion of variance not captured by the model.

$$S^2 = \frac{SCE}{Y_e} = \frac{\sum_{i=1}^{i=N} (Y_i - \bar{Y}_i)^2}{(N-P)} = \frac{0.0101568}{8} = 0.0012696 \tag{16}$$

### 4.5. Variance on one effect

This value is defined by the (17):

$$S_i^2 = \frac{S^2}{n} = \frac{0.0012696}{19} = 6.68211e^{-5} \tag{17}$$

The $t_i$ statistical test is established from relationship as in (18):

$$t_i = \frac{|a_i|}{S_i} \tag{18}$$

We recall that the equation which translates the micro-coil model is given by (19):

$$Y = 0.0893613 + 0.098459 * n - 1.02897e^{-8} * d_{out} + 0.0800561 * w + 0.0146402 * s + 2.13323e^{-9} * nd_{out} + 0.0797439 * nw + 0.0146098 * n_s + 5.96874e^{-11} * d_{out}w + (-)5.87277e^{-9} d_{out}s + 4.667e^{-9} w_s \tag{19}$$

As an example, the coefficient of the number of turns $n$, $t_n$= coefficient of the number of turns $n/Si = 0.0989459/0.0081279 = 12.7$. The mathematical model was determined from 19 tests and has 11 coefficients. Thus there are $\nu = 19 - 11 = 8$ degrees of freedom, the student table [23] gives. For a 5% risk with $\nu = 8$, $t_{crit}$ (0.05, 8) = 2.306. An effect will be significant at the 5% risk if the corresponding statistical test $t_{obs}$ is greater than 2.306. Thus, the $t_v$ effect of inductance is less than $t_{crit}$ and therefore not significant. Performing the same calculation for all variables gives the results as in Table 6.

Analysis of variance or ANOVA is employed to determine the threshold beyond which an effect is no longer statistically significant. The results indicate that four main effects and one interaction exhibit a probability of at least 95% of being significant. Although Table 6 raises some uncertainty regarding the influence of the inter-turn spacing, it should be noted that the ratio between the observed statistics ($t_{obs}$) associated with this effect and the critical value ($t_{crit}$) is equal to 85.42%. This indicates that the inter-turn effect is close to the significance threshold. as ($t_{obs}$) is nearly equal to ($t_{crit}$) (1.97 < 2.306).

Table 6. Analysis of the effects of the micro-coil mathematical model

| Variables | Effect | $t_{obs}$ | Results |
|---|---|---|---|
| $a_0$ | 0.0893 | 10.93>2.306 | Significant |
| The inter-turns $s$ | 0.0989 | 1.79 <2.306 | Significant |
| The width $t$ | 0 | 0 <2.306 | Not significant |
| The thickness $w$ | 0.0800 | 9.79>2.306 | Significant |
| The turnsnumber $n$ | 0.0146 | 12.10>2.306 | Significant |
| $n \times d_{out}$ | $3.469e^{-18}$ | 2.60964e-7<2.306 | Not significant |
| $n \times w$ | 0.0797 | 9.75>2.306 | Significant |
| $n \times s$ | 0.0146 | 1.78<2.306 | Not significant |
| $d_{out} \times w$ | 0 | 7.30173e-9<2.306 | Not significant |
| $d_{out} \times s$ | 0 | 7.18433 e-7<2.306 | Not significant |
| $w \times s$ | $-7.5e^{-10}$ | 5.70927 e-7<2.306 | Not significant |

These results clearly demonstrate that the inter-turn spacing ($s$), the thickness ($w$) and the number of turns ($n$) have a statistically significant influence on the inductance ($L$). Consequently, only these three factors along with the significant interaction ($n \times w$) should be considered in the optimization process aimed at increasing or decreasing the inductance as they exhibit a meaningful impact on the system response.

### 4.6. Confidence interval of model effects

Once the significant and insignificant effects have been determined the next step is to establish the confidence interval for the coefficients of the mathematical model. The confidence interval is expressed as (20).

$$a_i - t[(a.v)]S_i.a_i + t(a.v)S_i = [\mathrm{a_i} - 2.306 * 0.00817442.\mathrm{a_i} + 2.306 * 0.00817442] \quad (20)$$

Table 7 shows the confidence interval calculations for all the coefficients in the model. Table 7 confirms the results of Table 6. It is clear that, for example $a_o = 0.0893$ is significantly different from zero at the 5% risk whereas the second example the $d_{out}$*w interaction is not significantly different from zero at the same risk.

Table 7. Confidence intervals for mathematical model coefficients

| Model coefficient | Bottom limit | Upper limit |
|---|---|---|
| $a_o$ = 0.0893613 | 0.0893613 - 0.0188502 = 0.0705111 | 0.0893613 + 0.0188502 = 0.1082115 |
| $a_n$ = 0.0989459 | 0.08000957 | 0.1177961 |
| $ad_{outt}$ = -1.02897 e-008 | -0.0188502 | 0.0188502 |
| $a_w$ = 0.0800561 | 0.0612059 | 0.0989063 |
| $a_s$ = 0.0146402 | -0.00421 | 0.0334904 |
| $n \times d_{out}$ = 2.13323 e-009 | -0.0188502 | 0.0188502 |
| $n \times w$ = 0.079744 | 0.0608938 | 0.0985942 |
| $n \times s$ = 0.0146098 | -0.0042404 | 0.03346 |
| $d_{out} \times w$ = 5.96874 e-011 | -0.0188502 | 0.0188502 |
| $d_{out} \times s$ = -5.87277 e-009 | -0.0188502 | 0.0188502 |
| $w \times s$ = 4.667 e-009 | -0.0188502 | 0.0188502 |

Note: $t(a, \nu) = t(0.05, 8) = 2.306$ i.e., $a$=0.05=5% (tolerance or risk) and $\nu$=8 is the number of degrees of freedom of the residuals ∑(SCE).

### 4.7. Variance analysis

The statistical analysis of the model as a whole continues with the construction of a statistical test. The regression analysis table is used to group together the various stages leading to the statistical analysis of the inductance regression, as in Table 8. The Fisher-Sned table [23] gives for $\nu 1 = 10$ and $\nu 2 = 8$ $F_{crit} = 3.35$ for a risk of 5%. Given that ($F_{obs} = 26.37$) >($F_{crit} = 3.35$) we therefore accept the assumption that the model is linear.

Table 8. Inductance regression analysis

| Source | Sum of squares | Degree of liberty | Medium square | $F_{obs}$ |
|---|---|---|---|---|
| Model | $\text{SMC} = \sum(SCM)i = 0.36627961$ | 10 | $\frac{\text{SMC}}{10} = 0.036628$ | $\frac{\text{SMC}}{10} / \frac{SCE}{8} = 26.37$ |
| Residuals | $SCE = \sum(SCE)i = 0.01152109$ | 8 | $\frac{SCE}{8} = 0.00144$ | |
| Total | $\text{SCT} = SCM + SCE = 0.37780099$ | 18 | | |

### 4.8. Descriptive quality of the model

The regression analysis table can be used to immediately establish the coefficient of determination from (15)-(17).

$$R^2 = \frac{\text{SMC}}{\text{SCT}} = 1 - \frac{\text{SCE}}{\text{SCT}}$$
$$R^2\% = \frac{\text{SCM}}{\text{SCT}} * 100 = 97.31\% \quad (21)$$

When analysing test results, it is essential to avoid using the $R^2$ coefficient, instead the adjusted coefficient of determination $R^2_{ajust}$ should be used. The regression analysis table can be used to correct the coefficient defined in (23). The coefficient $R^2_{ajust}$ is then defined by:

$$R^2_{ajust} = 1 - \frac{\text{SCE}/(\text{N}-\text{P})}{\text{SCT}/(\text{N}-1)} \quad (22)$$

$SCE = 0.01152109$, $N = 19$, $P = 11$, $SCT = 0.037780$, SCE, SCM and SCT are calculated from Table 8.

$$R^2_{ajust}\% = \left(1 - \frac{\text{SCE}/(8)}{\text{SCT}/(18)}\right) = 93.95\% \quad (23)$$

### 4.9. Predictive quality of the model

By analogy with the coefficient of determination $R^2$, we define the coefficient $R^2$ predictive. also noted $Q^2$ from (20).

$$Q^2 = 1 - \frac{\text{Press}}{\text{SCT}} \quad (24)$$

The smaller the prediction error, the more predictive a model will be so we define the statistic, given by (19).

$$P_{ress} = \sum_{i=1}^{n} e_i^2 \quad (25)$$

As long as the value of $P_{ress}$ is low the postulated or well-established model is predictive.

$$P_{ress} = \sum_{i=1}^{n} e_i^2 = \sum_{i=1}^{19}(Y_i - \hat{Y})^2 \hat{\text{Y}}\text{: is the calculated column matrix. } \hat{Y} = \text{X. A} \quad (26)$$

$X$: matrix for calculating the effects of dimension (19, 11). This matrix represents the impact calculation matrix obtained from Table 3.

$$X = \begin{pmatrix}
1 & -1 & -1 & -1 & -1 & 1 & 1 & 1 & 1 & 1 & 1 \\
1 & 1 & -1 & -1 & -1 & -1 & -1 & -1 & 1 & 1 & 1 \\
1 & -1 & 1 & -1 & -1 & -1 & 1 & 1 & -1 & -1 & 1 \\
1 & 1 & 1 & -1 & -1 & 1 & -1 & -1 & -1 & -1 & 1 \\
1 & -1 & -1 & 1 & -1 & 1 & -1 & 1 & -1 & 1 & -1 \\
1 & 1 & -1 & 1 & -1 & -1 & 1 & -1 & -1 & 1 & -1 \\
1 & -1 & 1 & 1 & -1 & -1 & -1 & 1 & 1 & -1 & -1 \\
1 & 1 & 1 & 1 & -1 & 1 & 1 & -1 & 1 & -1 & -1 \\
1 & -1 & -1 & -1 & 1 & 1 & 1 & -1 & 1 & -1 & -1 \\
1 & 1 & -1 & -1 & 1 & -1 & -1 & 1 & 1 & -1 & -1 \\
1 & -1 & 1 & -1 & 1 & -1 & 1 & -1 & -1 & 1 & -1 \\
1 & 1 & 1 & -1 & 1 & 1 & -1 & 1 & -1 & 1 & -1 \\
1 & -1 & -1 & 1 & 1 & 1 & -1 & -1 & -1 & -1 & 1 \\
1 & 1 & -1 & 1 & 1 & -1 & 1 & 1 & -1 & -1 & 1 \\
1 & -1 & 1 & 1 & 1 & -1 & -1 & -1 & 1 & 1 & 1 \\
1 & 1 & 1 & 1 & 1 & 1 & 1 & 1 & 1 & 1 & 1 \\
1 & 0 & 0 & 0 & 0 & 0 & 0 & 0 & 0 & 0 & 0 \\
1 & 0 & 0 & 0 & 0 & 0 & 0 & 0 & 0 & 0 & 0 \\
1 & 0 & 0 & 0 & 0 & 0 & 0 & 0 & 0 & 0 & 0
\end{pmatrix}$$

$A$: matrix of coefficients for the model of dimension (11, 1). DIM (Ŷ)=(19, 1).

Ŷ: is the calculated column matrix. DIM (Ŷ)= (19, 1)

$$\hat{Y}=\begin{bmatrix} -0.0099. -0.0007. -0.0099. -0.0007. -0.0093.0.3189. \\ -0.0093.0.3189. -0.0099.0.0578. -0.0092.0.3774. \\ -0.0092.0.3774.0.0894.0.0894.0.0894 \end{bmatrix} \quad (27)$$

$Yi$: column matrix of DIM (19, 1) (that is the answer).

$$Yi=\begin{bmatrix} 1557e^{-5}.0.0092.1.557e^{-5}.0.0092.0.0006398. \\ 0.3288.0.006398.0.3288.7.6436e^{-5}.0.0677. \\ 7.6436e^{-5}.0.0677.0.0007.0.3873.0.0007 \\ 0.3873.0.035.0.038.0.036 \end{bmatrix} \quad (28)$$

The matrix calculation is too long and is done using a spreadsheet in Excel. The derivative error is calculated from a matrix product which gives (29).

$$P_{ress}=\sum_{i=1}^{19} e_i = 0.010021$$
$$Q^2 = 97.35\% \quad (29)$$

The closer the value of the ($Q^2$) coefficient is to 100%, the higher the predictive quality of the model. The value of ($Q^2$) obtained in this study indicates that the model is suitable for predicting responses within the investigated domain. In general, a robust mathematical model is characterized by values of ($R^2$) and ($Q^2$) close to unity with a coefficient of determination approaching one thereby reinforcing the validity and reliability of the model [24], [25]. For this first experimental design the calculated values of ($R^2$), ($Q^2$) and the adjusted coefficient of determination ($R^2_{adj}$) as in (30):

$$R^2 = 97.31\%$$
$$Q^2 = 97.35\%$$
$$R^2_{adj} = 93.95\% \quad (30)$$

The first-order model is adequate, the conclusion of this study is that the first-order model is largely satisfactory for interpreting the experimental values.

## 5. GRAPHICAL ANALYSIS OF THE MODEL

### 5.1. Model adequacy graph and measurement validation

The model adequacy plot provides a straightforward means of assessing the descriptive quality of the proposed model. This graphical representation compares the measured response values with those predicted by the model. The closer the distribution of points lies to the first bisector, the more satisfactory the model's descriptive performance as illustrated in Figure 3. In addition, the MODDE 05 software is used to verify the consistency of the experimental results and to identify any potentially anomalous or doubtful data points. The plot presented in Figure 4 indicates that all experimental results fall within the validation limits. There by confirming the reliability of the measurements and the adequacy of the model.

### 5.2. Iso-response curves

The MODDE 05 software also enables modeling based on RSM which can be used to facilitate the interpretation of the experimental design results, as in Figure 5. In the multidimensional space defined by variations in the micro-coil inductance ($L$) as a function of the geometric parameters (inter-turns $s$, width $t$, thickness $w$, number of turns $n$) the iso-response curves allow the identification of distinct regions corresponding to different classes of inductance values. In the ($w$, $s$) plane the inductance classes increase from 0.014 H to 0.166 H. indicating that both parameters contribute positively to the inductance. Similar trends are observed in the ($n$, $s$) and ($w$, $n$) planes. In the ($d_{out}$, $n$) plane a strong influence of both parameters is observed: increasing the outer diameter ($d_{out}$) from 150 µm to 500 µm results in a decrease in inductance from 0.173 H to 0.013 H. whereas increasing the number of turns ($n$) from 2 to 16 leads to an increase in inductance from 0.013 H to 0.173 H. Comparable behaviors are observed in the ($s$, $dout$) and ($w$, $d_{out}$) planes. Overall analysis of these response surfaces indicates that the parameters ($s$), ($n$), and ($w$) have a favorable contribution to the variation of the inductance ($L$).

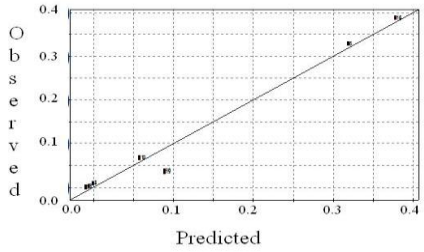


Figure 3. Model adequacy graph

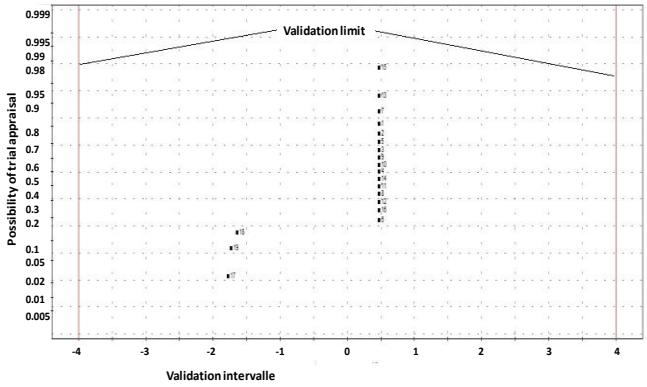


Figure 4. Test validation graph

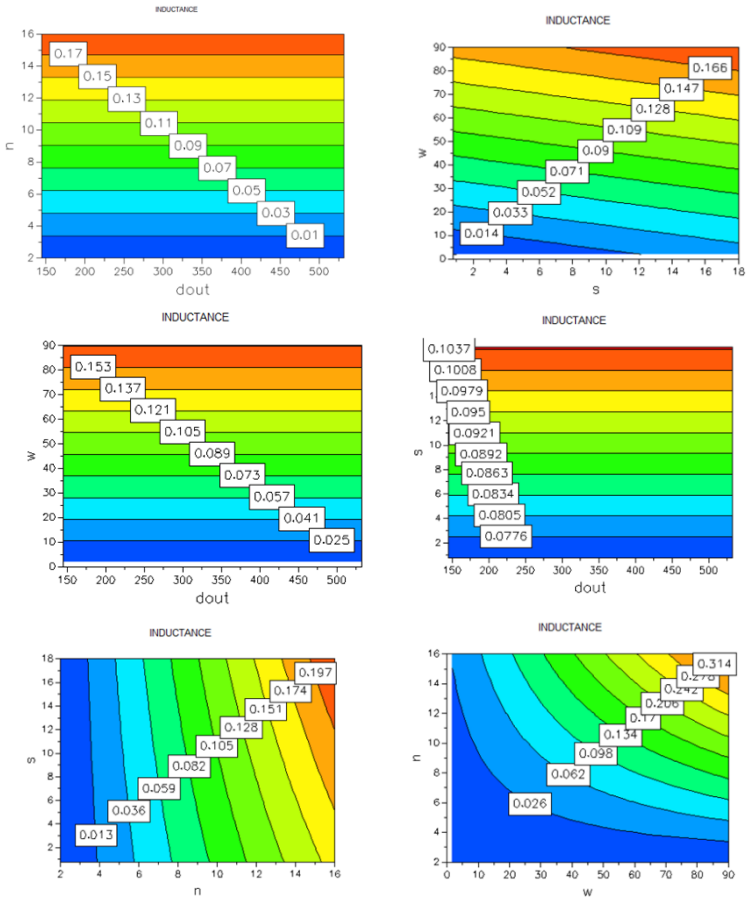


Figure 5. Modeling using *L* response surfaces and the influence of geometric parameters

### 5.3. Prediction curves

These curves show the predicted values plotted in black (central curve) which are statistically included in the interval between the blue and red curves with a tolerance interval generally equal to 5% as in Figure 6. It can also be seen that within the chosen ranges for each factor. The number of turn $n$, the turn spacing $s$ and the thickness $w$ are the most influential. They illustrate the influence of each factor on the inductance phenomenon. It is also need to be noteed that: the number of turn n has a positive effect: $L$ increases when $n$ increases; the thickness $w$ has a positive effect: $L$ increases when thickness $w$ increases; the spacing $s$ has a positive effect: $L$ increases when $s$ increases; and the external diameter $d_{out}$ has a negative effect: $L$ decreases as $d_{out}$ increases.

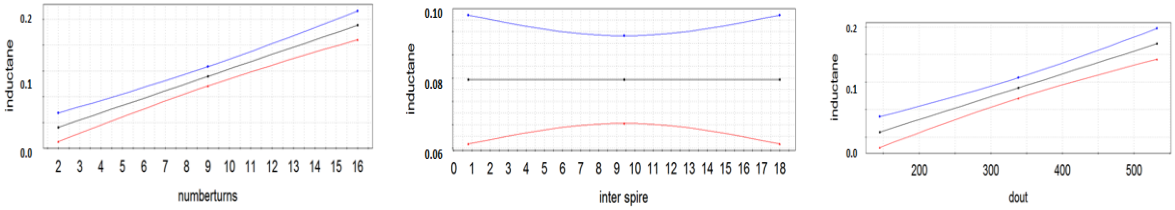


Figure 6. Prediction curves and influence of geometric factors on $L$

### 5.4. Response surface

The histogram in Figure 7 shows the difference between the estimated response (green) using the model and the response observed during the experiment (blue). From the analysis of this experimental design, it can be seen that a good performance was obtained because the two surfaces are very similar. It should be noted that the difference observed between them is due to the fact that the result obtained is purely experimental.

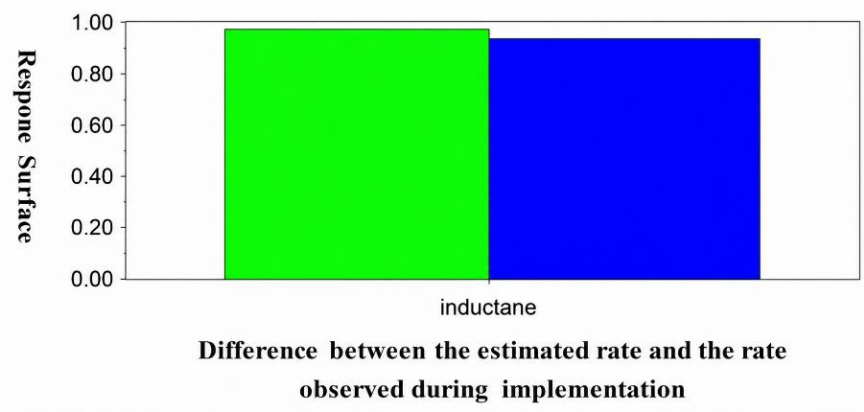


Figure 7. Illustration of the difference between the estimated rate and the rate observed during the experiment

## 6. CONCLUSION

The experimental analysis presented in this paper validates the proposed theoretical model. Tests conducted on various geometric parameters highlight the influence of inter-coil spacing as well as conductor width thickness s and outer diameter $d_{out}$ on the electrical characteristics of the micro-coil. The experimental results show that the width ($w$) is directly proportional to the inductance although it is inversely correlated with the outer diameter there by corroborating the fundamental design principles of integrated coils in the context of inductance modeling. The results obtained further strengthen the experimental conclusions and are consistent with theoretical predictions, although the influence of the outer diameter remains to be fully clarified. This study emphasizes the importance of experimental design methodologies in the analysis of inductive electrical characteristics. The systematic approach adopted facilitates both knowledge enhancement and effective capitalization of results. Moreover, this work illustrates the application of DOE techniques to a sizing problem that remains open to further investigation. It should be noted that the development of an

experimental design extends well beyond the simple construction of an experimental matrix from predefined templates. In conclusion it is essential to underline that the implementation of a design of experiments relies on specific modeling strategies tailored to the objectives of the study enabling an in-depth exploration of the experimental domain. The answers to the research questions are generally expressed through graphical representations. Although modern software tools greatly facilitate the interactive construction of experimental designs. It remains crucial to preserve methodological rigor and to maintain a sound experimental design philosophy.

This work presents an experimental approach based on the DOE methodology for the systematic analysis and optimization of square planar micro-coils. Unlike previous studies, it explicitly investigates interaction effects between key geometrical parameters and provides experimental validation of analytical models at the micrometer scale. The results demonstrate a strong agreement between simulations, theoretical predictions, and experimental measurements, confirming the accuracy of the proposed modeling approach. Additionally, the study evaluates the robustness of micro-coil performance with respect to fabrication-induced variations, providing insights for reliable design. However, the analysis is limited to single coil geometry and a frequency range centered around 500 kHz. Effects such as thermal behavior, the integration of magnetic materials, and full system-level interactions are not addressed, highlighting opportunities for future research.

## FUNDING INFORMATION

Authors state no funding involved.

## AUTHOR CONTRIBUTIONS STATEMENT

This journal uses the Contributor Roles Taxonomy (CRediT) to recognize individual author contributions, reduce authorship disputes, and facilitate collaboration.

| Name of Author | C | M | So | Va | Fo | I | R | D | O | E | Vi | Su | P | Fu |
|---|---|---|---|---|---|---|---|---|---|---|---|---|---|---|
| Assia Ouali | ✓ | ✓ | ✓ | ✓ | ✓ | ✓ | ✓ | ✓ | ✓ | ✓ | | | ✓ | |
| Fatima Zohra Medjaoui | ✓ | ✓ | ✓ | | | ✓ | ✓ | ✓ | ✓ | ✓ | ✓ | ✓ | | ✓ |
| Azzedine Hamid | ✓ | | ✓ | ✓ | ✓ | ✓ | ✓ | ✓ | | ✓ | ✓ | | ✓ | ✓ |
| Mohamed Rizouga | ✓ | | ✓ | | | | ✓ | | ✓ | | | ✓ | ✓ | |
| Abderrahim Mokhefi | | ✓ | ✓ | ✓ | ✓ | ✓ | ✓ | ✓ | | ✓ | ✓ | | ✓ | |
| Hocine Guentri | ✓ | ✓ | | | ✓ | | ✓ | | ✓ | | | ✓ | ✓ | |

C : **C**onceptualization
M : **M**ethodology
So : **So**ftware
Va : **Va**lidation
Fo : **Fo**rmal analysis
I : **I**nvestigation
R : **R**esources
D : **D**ata Curation
O : Writing - **O**riginal Draft
E : Writing - Review & **E**diting
Vi : **Vi**sualization
Su : **Su**pervision
P : **P**roject administration
Fu : **Fu**nding acquisition

## CONFLICT OF INTEREST STATEMENT

Authors state no conflict of interest.

## DATA AVAILABILITY

The authors declare that all data existing in this paper are available and can be made available to the publisher. Please contact T. A. the principal author of this paper.

## REFERENCES

[1] F. Z. Medjaoui, A. Hamid, Y. Guettaf, P. Spiteri, and V. Bley, "Conception and Manufacturing of a Planar Inductance on NiFe Substrate," *Transactions on Electrical and Electronic Materials*, vol. 20, no. 3, pp. 269–279, 2019, doi: 10.1007/s42341-019-00105-x.

[2] M. R. Benzidane *et al.*, "Miniaturization and Optimization of a DC–DC Boost Converter for Photovoltaic Application by Designing an Integrated Dual-Layer Inductor Model," *Transactions on Electrical and Electronic Materials*, vol. 23, no. 5, pp. 462–475, 2022, doi: 10.1007/s42341-021-00370-9.

[3] M. Derkaoui and Y. Benhadda, "Integrated Square On-Chip Inductor for Photovoltaic Converter Applications," *Journal of Renewable Energies*, no. Special Issue, pp. 3–11, 2023, doi: 10.54966/jreen.v1i1.1168.

[4] K. Benamer, A. Hamid, E. Rossi di Schio, A. Mokhefi, R. Melati, and P. Valdiserri, "Magnetic and Thermal Behavior of a Planar

Toroidal Transformer," *Energies* , vol. 17, no. 11, 2024, doi: 10.3390/en17112454.
[5] M. Li, C. Wang, Z. Ouyang, and M. A. E. Andersen, "Optimal Design of a Matrix Planar Transformer in an LLC Resonant Converter for Data Center Applications," *IEEE Journal of Emerging and Selected Topics in Power Electronics*, vol. 11, no. 2, pp. 1778–1787, 2023, doi: 10.1109/JESTPE.2022.3215623.
[6] R. E. A. Azim, "A Review of Tunable Inductors for Power Electronics: Techniques and Applications," *e-Prime - Advances in Electrical Engineering, Electronics and Energy*, vol. 9, 2024, doi: 10.1016/j.prime.2024.100655.
[7] S. Abi and B. Benhala, "Optimal Sizing of Integrated Inductor using a Hybrid Optimization Algorithm," in *2022 2nd International Conference on Innovative Research in Applied Science, Engineering and Technology, IRASET 2022*, 2022. doi: 10.1109/IRASET52964.2022.9737884.
[8] M. Eslamian, M. Kharezy, and T. Thiringer, "An Accurate Analytical Method for Leakage Inductance Calculation of Shell-Type Transformers with Rectangular Windings," *IEEE Access*, vol. 9, pp. 72647–72660, 2021, doi: 10.1109/ACCESS.2021.3080242.
[9] R. Hou *et al.*, "Optimization and Design of LCC Resonant High-Voltage Wide Range Power Supply for Magnetrons," *IEEE Journal of Emerging and Selected Topics in Power Electronics*, vol. 12, no. 4, pp. 3835–3847, Aug. 2024, doi: 10.1109/JESTPE.2024.3412800.
[10] Y. Liu, Z. Zhu, X. Liu, Q. Lu, X. Yin, and Y. Yang, "Physics based scalable inductance model for three-dimensional solenoid inductors," *Microelectronics Journal*, vol. 103, 2020, doi: 10.1016/j.mejo.2020.104867.
[11] R. Heikkinen, J. Sipilä, V. Ojalehto, and K. Miettinen, "Flexible data driven inventory management with interactive multi-objective lot size optimisation," *International Journal of Logistics Systems and Management*, vol. 46, no. 2, pp. 206–235, 2023, doi: 10.1504/IJLSM.2023.134404.
[12] L. Zhao, Y. Lyu, F. Liu, Z. Liu, and Z. Zhao, "Experimental Investigation on the Effect of Coil Shape on Planar Eddy Current Sensor Characteristic for Blade Tip Clearance," *Sensors*, vol. 24, no. 18, 2024, doi: 10.3390/s24186133.
[13] Y. Benazzouz and D. Guendouz, "A computer vision approach with OpenCV and deep learning for determining inductance in planar coils," *Military Technical Courier/Vojnotehnicki glasnik*, vol. 72, no. 4, pp. 1645–1670, 2024, doi: 10.5937/vojtehg72-51477.
[14] J. Bian, W. Zhang, Z. Shen, S. Li, and Z. Chen, "Analysis and optimization of mechanical properties of recycled concrete based on aggregate characteristics," *Science and Engineering of Composite Materials*, vol. 28, no. 1, pp. 516–527, 2021, doi: 10.1515/secm-2021-0050.
[15] G. Hancu, S. Orlandini, L. A. Papp, A. Modroiu, R. Gotti, and S. Furlanetto, "Application of experimental design methodologies in the enantioseparation of pharmaceuticals by capillary electrophoresis: A review," *Molecules*, vol. 26, no. 15, 2021, doi: 10.3390/molecules26154681.
[16] H. J. Leplaa, J. A. Tönjes, M. Bouterse, K. F. B. Soppe, and I. Klugkist, "Applying qualitative methods to experimental designs: A tutorial for the behavioral sciences," *PLOS One*, vol. 20, no. 6, Jun. 2025, doi: 10.1371/journal.pone.0324936.
[17] D. B. Ahire, V. J. Gond, and J. J. Chopade, "Geometrical parameter optimization of planner square-shaped printed spiral coil for efficient wireless power transfer system to biomedical implant application," *e-Prime - Advances in Electrical Engineering, Electronics and Energy*, vol. 2, 2022, doi: 10.1016/j.prime.2022.100045.
[18] Y. Liu, X. Liu, Q. Lu, T. Zhang, and X. Yin, "A T-Model with Parameter Extraction Method for Modeling 3-D Spiral Inductor," *IEEE Microwave and Wireless Components Letters*, vol. 32, no. 1, pp. 37–40, 2022, doi: 10.1109/LMWC.2021.3115127.
[19] S. G. Thottempudi *et al*., "Mathematical Optimization of Coil Geometries for Position Sensors," *Lecture Notes in Networks and Systems. Springer Nature Singapore*, pp. 569–588, 2025. doi: 10.1007/978-981-96-6429-0_45.
[20] A. Lalla, P. Di Barba, S. Hausman, and M. E. Mognaschi, "Deep Neural Network-Based Design of Planar Coils for Proximity Sensing Applications," *Sensors*, vol. 25, no. 14, 2025, doi: 10.3390/s25144429.
[21] A. Faria, L. Marques, L. Vale, C. Ferreira, F. Alves, and J. Cabral, "Analytical tool for optimization of position sensors based on eddy currents effect," *Heliyon*, vol. 8, no. 12, p. e11920, Dec. 2022, doi: 10.1016/j.heliyon.2022.e11920.
[22] I. E. Achouri, T. Zeghloul, G. Richard, K. Medles, H. Nouri, and L. Dascalescu, "Factors that influence the performance of a two-rotating disks-type tribo-aero-electrostatic separator for micronized WEEE," *IEEE Transactions on Industry Applications*, vol. 55, no. 1, pp. 802–811, 2019, doi: 10.1109/TIA.2018.2866546.
[23] N. Asprion *et al.*, "Implementation and Application of Model-Based Design of Experiments in a Flowsheet Simulator," *Journal of Chemical & Engineering Data*, vol. 65, no. 3, pp. 1135–1145, Mar. 2020, doi: 10.1021/acs.jced.9b00494.
[24] Y. J. Park, J. Kim, K. Na, K. Yang, and K. Cho, "Optimization and analysis of multilayer planar spiral coils for the application of magnetic resonance wireless power transfer to wearable devices," *Energies*, vol. 14, no. 16, 2021, doi: 10.3390/en14165113.
[25] B. Afsar, J. Silvennoinen, F. Ruiz, A. B. Ruiz, G. Misitano, and K. Miettinen, "An experimental design for comparing interactive methods based on their desirable properties," *Annals of Operations Research*, vol. 338, no. 2–3, pp. 835–856, 2024, doi: 10.1007/s10479-024-05941-6.

## BIOGRAPHIES OF AUTHORS

**Assia Ouali** obtained her degree in Electrical Engineering from the University of Science and Technology of Oran (USTO), Algeria in 2000, a Master's degree in Modeling and Computer-Aided Design in 2005. and a Ph.D. in Electrical Engineering in 2013 with a thesis entitled: 3D modeling of end effects in the frontal parts of induction machines using 2D and 3D finite element software. She has been a professor of Electrical Machines and Magnetic fields in the Department of Electrical Engineering at the University of Science and Technology of Oran since 2006. She is a member of the LEPA Research Laboratory (Applied Power Electronics Laboratory). She can be contacted at email: ouali.assia31000@gmail.com, assia.ouali@univ-usto.dz.

**Fatima Zohra Medjaoui** obtained her degree in Electrical Engineering from the University of Science and Technology of Oran (USTO) in 1990, Master's degree in Electrical Discharges in 2006, and a Ph.D. in Integrationfor Power Electronics in 2019. She is currently a senior lecturer and member of the Applied Power Electronics Research Laboratory on Integration for Power Electronics and Materials in the Electrical Engineering Department at USTO. Her current research focuses onthe integration of passive components for low-power electronics for power converter topologies, renewable energies and energy efficiency. She can be contacted at email: medjaouifaz@yahoo.fr, fatimazohra.medjaoui@univ-usto.dz.

**Azzedine Hamid** obtained his degree in Electrical Engineering from the University of Science and Technology of Oran (USTO) in 1987, a Master's degree in Electrical Discharges in 1994, and a Ph.D. in Dielectric Materials in 2005. He is currently a professor and member of the Applied Power Electronics Research Laboratory and team leader of Integration for Power Electronics and Materials in the Electrical Engineering Department at USTO. His current research focuses on the integration of passive components for low-power electronics for power converter topologies, renewable energies and energy efficiency. He can be contacted at email: a.hamid@cu-elbayadh.dz.

**Mohamed Rizouga** obtained his degree in Electrical Engineering from the University of Science and Technology of Oran (USTO) in 1988, Master's degree by Passing High Voltage Insulators in 1991, and a Ph.D. in Dielectric Materials and High Voltage in 2008. He is currently a professor and member of the Applied Power Electronics Research Laboratory of Integration for Power Electronics and Materials in the Electrical Engineering Department at USTO. His current research interests include the integration of passive components and the electrostatic separation of granular materials. He can be contacted at email: Rezouga2@yahoo.fr, mohamed.rizouga@univ-usto.dz.

**Abderrahim Mokhefi** was born in 1992 in Oran, Algeria. He received his Bachelor's and Master's degrees in Transportation and Distribution of Hydrocarbons from the University of Boumerdes in Algeria. He is currently a doctor of Energy Mechanics from Bechar University and a teacher of mathematics and numerical methods at the Faculty of Electrical Engineering. His current research interests are mainly in the field of nano technology, computational fluid dynamics, electromagnetic field theory and magnetohydrodynamic. He can be contacted at email: abderahimmokhefi@yahoo.fr.

**Hocine Guentri** in 1996, he graduated from the Department of Electrotechnics of the Faculty of Electrical Engineering at the University Ibn Khaldun in Algeria. The Master's degree from the University of Saida Algeria. The Ph.D. degree from the University of Sidi Bel-Abbes, Algeria, in 2018.His research activities primarily concentrate on power systems, FACTS, renewable energy, and sustainable energy, and his research activities focus on smart grid systems and storage hybrid systems. He is a lecturer at the university centre Nour Bachir El Bayadh in Algeria. He can be contacted at email: h.guentri@cu-elbayadh.dz.